



Coronavirus Endoribonuclease Activity in Porcine Epidemic Diarrhea Virus Suppresses Type I and Type III Interferon Responses

Xufang Deng,^a Albert van Geelen,^b Alexandra C. Buckley,^b Amornrat O'Brien,^a Angela Pillatzki,^c Kelly M. Lager,^b Kay S. Faaberg,^b  Susan C. Baker^a

^aDepartment of Microbiology and Immunology, Loyola University Chicago, Stritch School of Medicine, Maywood, Illinois, USA

^bVirus and Prion Research Unit, USDA-ARS-National Animal Disease Center, Ames, Iowa, USA

^cAnimal Disease Research & Diagnostic Laboratory, South Dakota State University, Brookings, South Dakota, USA

ABSTRACT Identifying viral antagonists of innate immunity and determining if they contribute to pathogenesis are critical for developing effective strategies to control emerging viruses. Previously, we reported that an endoribonuclease (EndoU) encoded by murine coronavirus plays a pivotal role in evasion of host innate immune defenses in macrophages. Here, we asked if the EndoU activity of porcine epidemic diarrhea coronavirus (PEDV), which causes acute diarrhea in swine, plays a role in antagonizing the innate response in porcine epithelial cells and macrophages, the sites of viral replication. We constructed an infectious clone of PEDV-Colorado strain (icPEDV-wt) and an EndoU-mutant PEDV (icPEDV-EnUmt) by changing the codon for a catalytic histidine residue of EndoU to alanine (His226Ala). We found that both icPEDV-wt and icPEDV-EnUmt propagated efficiently in interferon (IFN)-deficient Vero cells. In contrast, the propagation of icPEDV-EnUmt was impaired in porcine epithelial cells (LLC-PK1), where we detected an early and robust transcriptional activation of type I and type III IFNs. Infection of piglets with the parental Colorado strain, icPEDV-wt, or icPEDV-EnUmt revealed that all viruses replicated in the gut and induced diarrhea; however, there was reduced viral shedding and mortality in the icPEDV-EnUmt-infected animals. These results demonstrate that EndoU activity is not required for PEDV replication in immortalized, IFN-deficient Vero cells, but is important for suppressing the IFN response in epithelial cells and macrophages, which facilitates replication, shedding, and pathogenesis *in vivo*. We conclude that PEDV EndoU activity is a key virulence factor that suppresses both type I and type III IFN responses.

IMPORTANCE Coronaviruses (CoVs) can emerge from an animal reservoir into a native host species to cause pandemic respiratory or gastrointestinal diseases with significant mortality in humans or domestic animals. Porcine epidemic diarrhea virus (PEDV), an alphacoronavirus (alpha-CoV), infects gut epithelial cells and macrophages, inducing diarrhea and resulting in high mortality in piglets. How PEDV suppresses the innate immune response was unknown. We found that mutating a viral endoribonuclease, EndoU, results in a virus that activates both the type I interferon response and the type III interferon response in macrophages and epithelial cells. This activation of interferon resulted in limited viral replication in epithelial cell cultures and was associated with reduced virus shedding and mortality in piglets. This study reveals a role for EndoU activity as a virulence factor in PEDV infection and provides an approach for generating live-attenuated vaccine candidates for emerging coronaviruses.

KEYWORDS coronavirus, endoribonuclease, immune evasion, interferon antagonist, porcine epidemic diarrhea virus, type I interferon, type III interferon

Citation Deng X, van Geelen A, Buckley AC, O'Brien A, Pillatzki A, Lager KM, Faaberg KS, Baker SC. 2019. Coronavirus endoribonuclease activity in porcine epidemic diarrhea virus suppresses type I and type III interferon responses. *J Virol* 93:e02000-18. <https://doi.org/10.1128/JVI.02000-18>.

Editor Susana López, Instituto de Biotecnología/UNAM

Copyright © 2019 American Society for Microbiology. All Rights Reserved.

Address correspondence to Kay S. Faaberg, kay.faaberg@ars.usda.gov, or Susan C. Baker, sbaker1@luc.edu.

Received 8 November 2018

Accepted 25 January 2019

Accepted manuscript posted online 6 February 2019

Published 3 April 2019

Viruses have evolved a myriad of strategies to overcome host innate antiviral defenses for successful infections. Previous studies identified viral factors that target key players in the signaling pathways responsible for activating the type I interferon (IFN) response, as well as viral factors that target the downstream signaling pathways needed to amplify IFN-stimulated genes (ISGs) that induce an antiviral state (1, 2). For pathogens that replicate in respiratory or gut epithelial cells, the type III IFN response mediated by IFN lambda (IFN- λ) represents the first line of defense that must be mitigated (3–5). Identifying viral antagonists and investigating how these viral factors interrupt or delay innate responses is important for controlling viral pathogenesis and developing new targets for therapeutics and new designs for live-attenuated vaccines.

Coronaviruses (CoVs) are enveloped, positive-sense RNA viruses that are well known for their ability to emerge from animal reservoirs, particularly bats, and make the jump into a new species, as seen with severe acute respiratory syndrome CoV (SARS-CoV) and Middle East respiratory syndrome CoV (MERS-CoV) (6, 7). CoVs primarily infect lung and gut epithelial cells, resulting in respiratory and enteric diseases, respectively. CoVs are also notorious for their ability to delay the innate immune response to infection, which can contribute to disease severity and potentially contribute to persistence (8). As CoVs have tropism for primary epithelial cells, these viruses must be equipped with strategies to abate the innate response generated in the epithelium. Epithelial cells, unlike myeloid immune cells, such as macrophages and dendritic cells, generate and respond to type III IFNs (9, 10). However, how CoVs modulate the type III IFN-mediated antiviral defense in the primary epithelium is not clear.

CoVs belong to the family *Coronaviridae* of the order *Nidovirales* and have four genera: *Alphacoronavirus*, *Betacoronavirus*, *Gammacoronavirus*, and *Deltacoronavirus*. These viruses have the longest known RNA genomes (~30 kb) (Fig. 1A), which encode 15 to 16 nonstructural proteins (nsp1 through nsp16), four structural proteins (spike [S], envelope [E], membrane [M], and nucleocapsid [N]), and a variety of strain-specific accessory proteins. Many betacoronavirus (beta-CoV) accessory proteins and several nsps have been identified as IFN antagonists (11). Recently, we and others added a new member to the list of CoV IFN antagonists, nsp15/EndoU (12–14). Coronavirus nsp15 was identified as an endoribonuclease (15, 16), but it is now clear that endoribonuclease activity is not required for viral RNA synthesis, since viruses with mutations in the catalytic sites required for EndoU activity replicate efficiently in IFN-deficient cells (12, 13, 17). However, EndoU activity plays a pivotal role in evading host sensing of viral double-stranded RNA (dsRNA). Inactivating EndoU catalytic activity resulted in robust and early induction of type I IFN in virus-infected mouse macrophages, rapid clearance of infectious virus from the liver and spleen in infected mice, and the generation of a protective immune response. Since nsp15/EndoU is highly conserved across all CoVs (Fig. 1B), we sought to determine if the IFN antagonism we detected in murine CoV is conserved in other CoVs, especially those that target epithelial cells. In the present study, we sought to characterize the role of EndoU of an enteric CoV, porcine epidemic diarrhea virus (PEDV).

PEDV emerged suddenly in the United States in 2013, causing devastating losses in swine production (18–20). Despite early efforts to provide protection with killed or subunit vaccines, there is not yet an effective modified live vaccine (21, 22). PEDV is an alphacoronavirus (alpha-CoV) that infects the enteric tract of swine and causes diarrhea (19, 23). This virus is highly pathogenic in neonatal pigs (up to 100% mortality), and the mortality inversely correlates with the age of the animal. PEDV infection occurs primarily in intestinal epithelial cells (enterocytes), but it can also be detected in the macrophage-like cells located within Peyer's patches (24–26). Since epithelial cells primarily make and respond to type III IFN, while macrophages primarily respond to type I IFN, we asked if a CoV IFN antagonist can modulate both of these activities. Here, we report that the EndoU activity of PEDV not only antagonized the type I IFN response in porcine macrophages but also inhibited the type III IFN response in porcine epithelial cells, which may facilitate replication, shedding, and disease in piglets.

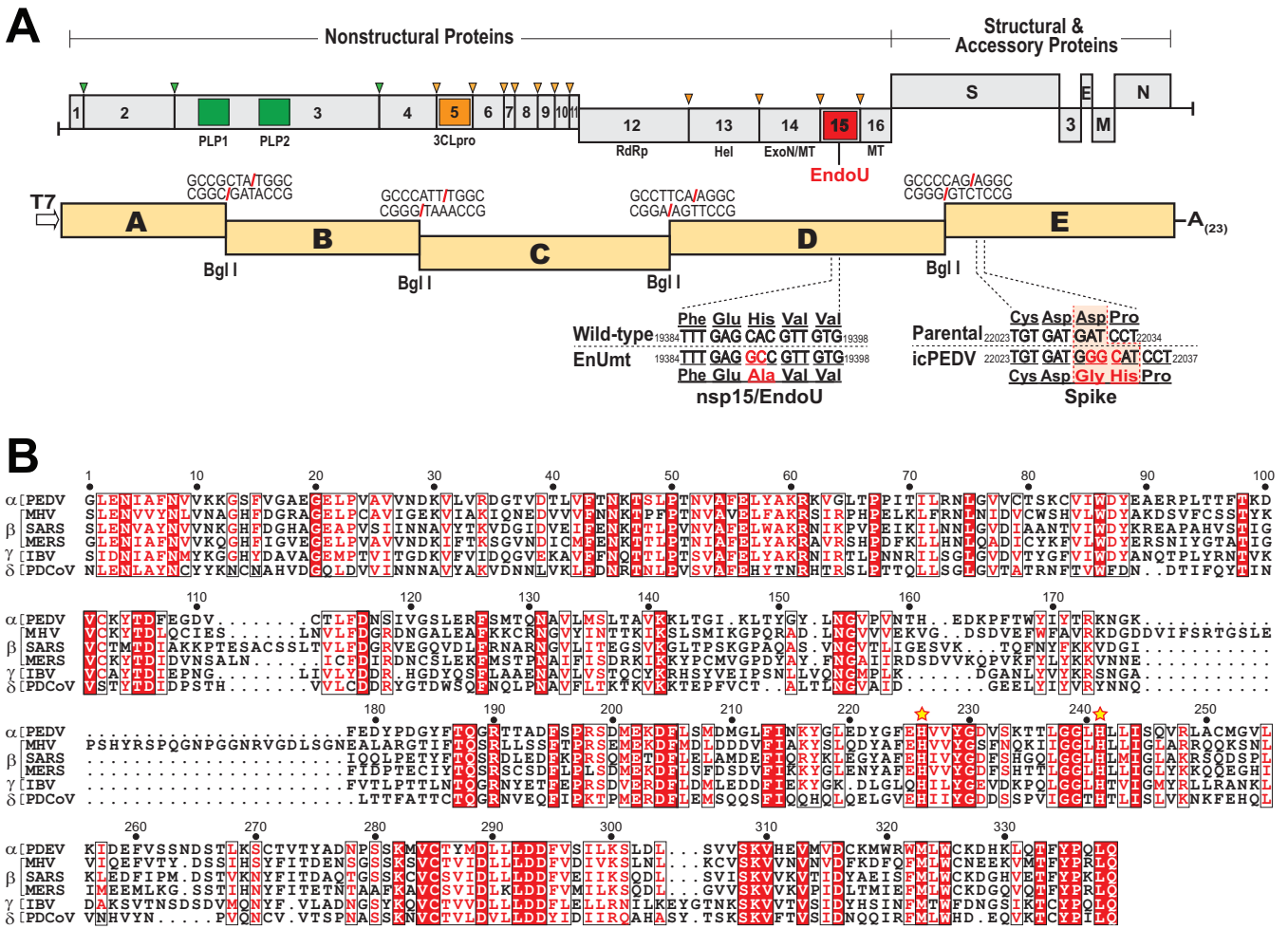


FIG 1 Schematic diagram of the strategy used to generate an infectious clone of the Colorado strain of PEDV and amino acid homology of the EndoU domain of coronaviruses. (A) PEDV replicase polyprotein, structural, and accessory components, with viral proteases and predicted cleavage sites (triangles). PLP, papain-like proteases; 3CLpro, 3C-like protease; RdRp, RNA-dependent RNA polymerase; Hel, helicase; ExoN/MT, exoribonuclease/guanosine-N7-methyltransferase; EndoU, endoribonuclease; MT, O-methyltransferase; S, spike; 3, open reading frame (ORF) 3; E, envelope; M, membrane; N, nucleocapsid. The 5 DNA fragments with restriction enzyme sites used for ligation are depicted with the mutations described in this study. (B) Sequence alignment of CoV nsp15/EndoU. The catalytic histidine residues are indicated with yellow stars. MHV, mouse hepatitis virus; SARS, severe acute respiratory syndrome CoV; MERS, Middle East respiratory syndrome CoV; IBV, infectious bronchitis virus; PDCoV, porcine deltacoronavirus.

RESULTS

Generating an infectious clone of PEDV-Colorado strain and an EndoU-mutant PEDV.

To investigate if PEDV EndoU acts as an IFN antagonist in porcine cells, we generated an infectious clone of PEDV and an EndoU-deficient mutant virus using a previously described strategy (27) with minor modifications (Fig. 1, see details in Materials and Methods). Briefly, three synthetic DNA fragments were generated based on the PEDV-Colorado genomic RNA sequence (28). These synthetic DNAs were used as the template for PCR amplification of five segments that were then cloned into plasmid vector backbones. The promoter sequence of T7 RNA polymerase and a poly(A) tail were inserted at the 5' and 3' ends of the genome, respectively. In addition, the sequence of the N gene was amplified and cloned into a pCDNA3.1 vector that carries a T7 promoter sequence. To rescue the virus, the five PEDV DNA fragments were digested from their vectors and ligated *in vitro*. The ligated DNA and linearized N gene plasmid DNA were used as the templates for *in vitro* RNA transcription reactions to yield full-length genomic RNA and N gene transcripts. These RNA transcripts were mixed and coelectroporated into Vero cells, where they were translated into viral proteins to initiate the replication and assembly of infectious particles of PEDV. Initially, no

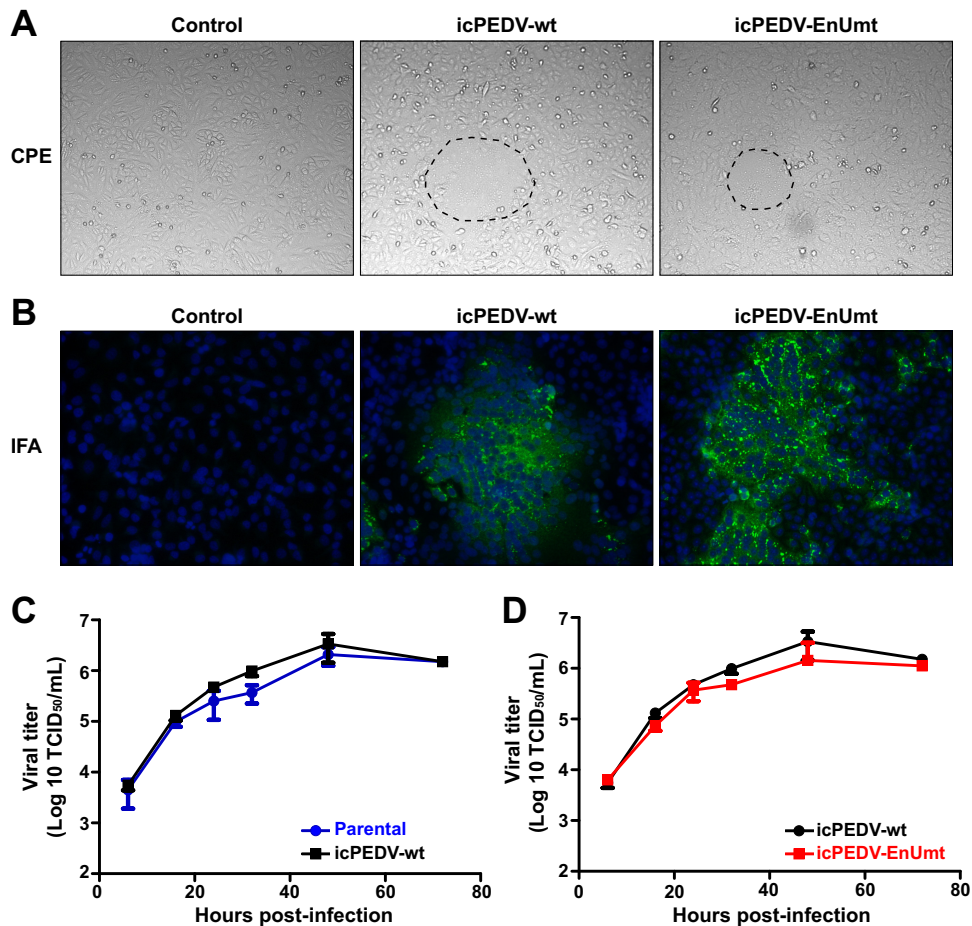


FIG 2 Recovery of an infectious clone of the Colorado strain of PEDV wild type (icPEDV-wt) and EndoU mutant (icPEDV-EnUmt). (A) Vero cells were electroporated with *in vitro* transcribed PEDV RNA and characteristic CPE was observed at 30 h postelectroporation in the presence of 2 μ g/ml TPCK-treated trypsin. (B) Vero cells infected with supernatant from electroporated cells were fixed at 24 hpi and probed with fluorescein isothiocyanate (FITC)-conjugated monoclonal anti-N antibody (green) and Hoechst dye for nuclei DNA (blue) by immunofluorescence assay (IFA). (C and D) Growth kinetics of parental strain, wild-type, and EndoU mutant PEDV in Vero cells. Supernatants from infected cells were collected at indicated time points and the titers were determined on Vero cells. TCID₅₀ was calculated using the Reed-Muench method (59).

syncytia-like cytopathic effects (CPE) were observed in the electroporated cells, nor were CPE detected upon passage of the supernatant from the electroporated cells. However, using reverse transcription-PCR (RT-PCR), we detected viral leader-containing subgenomic mRNA from the total RNA isolated from electroporated cells, indicating that virus replication was occurring (data not shown). Similar results were reported during the generation of the infectious clone of PEDV-PC22A, with no CPE detected in cell culture but with clear evidence of virus production, since supernatant could be used to induce disease in piglets (29). For PEDV-PC22A, Hou et al. found that insertion of a trinucleotide into the spike sequence, resulting in replacement of aspartic acid by a glycine residue, and the addition of a histidine residue (D466GH), resulted in development of CPE during PEDV infection in Vero cells (30). Since the Colorado and PC22A strains share 99% identity in the spike region, we reasoned that introducing the D466GH mutation into the spike sequence of the Colorado strain spike sequence would induce CPE in Vero cells. As expected, within 24 to 48 h postelectroporation, syncytia-like CPE was detected in Vero cells electroporated with the *in vitro* synthesized RNA (Fig. 2A). The virus recovered from the supernatant was designated infectious clone wild type, icPEDV-wt. Similarly, we generated an EndoU-deficient mutant, designated icPEDV-EnUmt, by introducing a His-to-Ala substitution (H226A) of the catalytic residue

of nsp15 (Fig. 1). These viruses were passaged in Vero cells, and the expression of N protein was detected by immunofluorescence using fluorescein isothiocyanate (FITC)-conjugated anti-N monoclonal antibody (Fig. 2B). The genome sequence of each virus was confirmed by Illumina high-throughput sequencing of RNA isolated from virus particles. The consensus sequence was found to have no additional mutations other than those described above.

Evaluating replication of icPEDV-wt and icPEDV-EnUmt. Since the recombinant PEDV wild type (icPEDV-wt) had a D466GH mutation in the spike protein, we wanted to determine if this mutation would affect viral replication in cell culture. To address this, we compared the replication kinetics of the parental strain and icPEDV-wt in Vero cells over 80 h. The results show that icPEDV-wt exhibited similar replication kinetics to those of the parental Colorado strain (Fig. 2C), indicating that the change in the spike sequence did not alter PEDV replication in Vero cells. This result is consistent with the findings of Hou et al. (30). We also found that icPEDV-EnUmt replicated as efficiently as icPEDV-wt in Vero cells (Fig. 2D), demonstrating that EndoU activity is not required for PEDV replication in Vero cells, an IFN-deficient, immortalized cell line.

Evaluating the kinetics of activating type I and type III interferons in PEDV-infected PK1 cells. Porcine kidney epithelial cells, LLC-PK1 (ATCC CL101), termed PK1 cells, are a porcine kidney epithelial cell line that has been used for isolating and propagating porcine CoVs (31) and are permissive to PEDV infection (32). To determine if this cell line can sense and respond to dsRNA, we transfected these cells with a dsRNA mimic, poly(I:C). We detected significant transcriptional expression of IFN- β and IFN- λ 3 mRNA (Fig. 3A) and ISGs (Fig. 3B) at 16 h posttransfection, compared to that in mock-transfected cells. These results demonstrate that PK1 cells are capable of detecting and responding to cytoplasmic dsRNA molecules. Next, we evaluated the kinetics of IFN activation after infection with icPEDV-wt or icPEDV-EnUmt. PK1 cells were mock-infected or infected with the indicated virus at a dose of 0.1 tissue culture infectious dose 50 (TCID₅₀) per cell. The mRNA levels of IFN- β , IFN- λ 3, the PEDV nucleocapsid (N) gene, and the porcine glyceraldehyde-3-phosphate dehydrogenase (GAPDH) gene were evaluated using reverse transcription-quantitative PCR (RT-qPCR) at different hours postinfection (hpi) (8, 12, 24, and 32 hpi). We found that in icPEDV-wt-infected cells, the relative mRNA level of IFN- λ 3 was not significantly changed at the tested time points, and the IFN- β mRNA was detected at a low level until late time points of infection (24 and 32 hpi). In contrast, icPEDV-EnUmt infection activated an earlier and more robust IFN response, as revealed by elevated levels of IFN- β mRNA as early as 8 hpi, and IFN- λ 3 at 24 hpi (Fig. 3C and D). We also evaluated viral replication by monitoring levels of PEDV N gene mRNA and production of progeny virus. The N gene mRNA expression in icPEDV-EnUmt-infected cells was significantly reduced at late times postinfection (24 and 32 hpi) (Fig. 3E). We found a significantly reduced titer of icPEDV-EnUmt at 32 and 48 hpi, compared to those for icPEDV-wt (Fig. 3F).

To determine if the elevated IFN expression could stimulate robust activation of an antiviral response, we evaluated the expression of ISGs and proinflammatory cytokines in virus-infected PK1 cells. As shown in Fig. 4, icPEDV-EnUmt infection stimulated an earlier and more robust transcriptional activation of ISGs and proinflammatory cytokines as revealed by activation of ISG54, ISG15, 2'-5'-oligoadenylate synthetase 1 (OAS1) and tumor necrosis factor alpha (TNF- α) (Fig. 4A to D). Taken together, these results indicate that the EndoU activity of PEDV nsp15 is important for inhibiting type I and III IFN responses, which facilitates viral replication in IFN-competent cells.

IFN production in porcine macrophages infected with PEDV. PEDV replication can be detected in macrophage-like cells within Peyer's patches and lymph nodes of infected animals (24–26). PEDV has also been shown to infect primary porcine alveolar macrophages (PAMs) *in vitro*, although replication is minimal in these cultured cells (33). Therefore, to determine if EndoU activity plays a role in controlling the IFN response in primary macrophages, we infected PAMs with either icPEDV-wt or icPEDV-

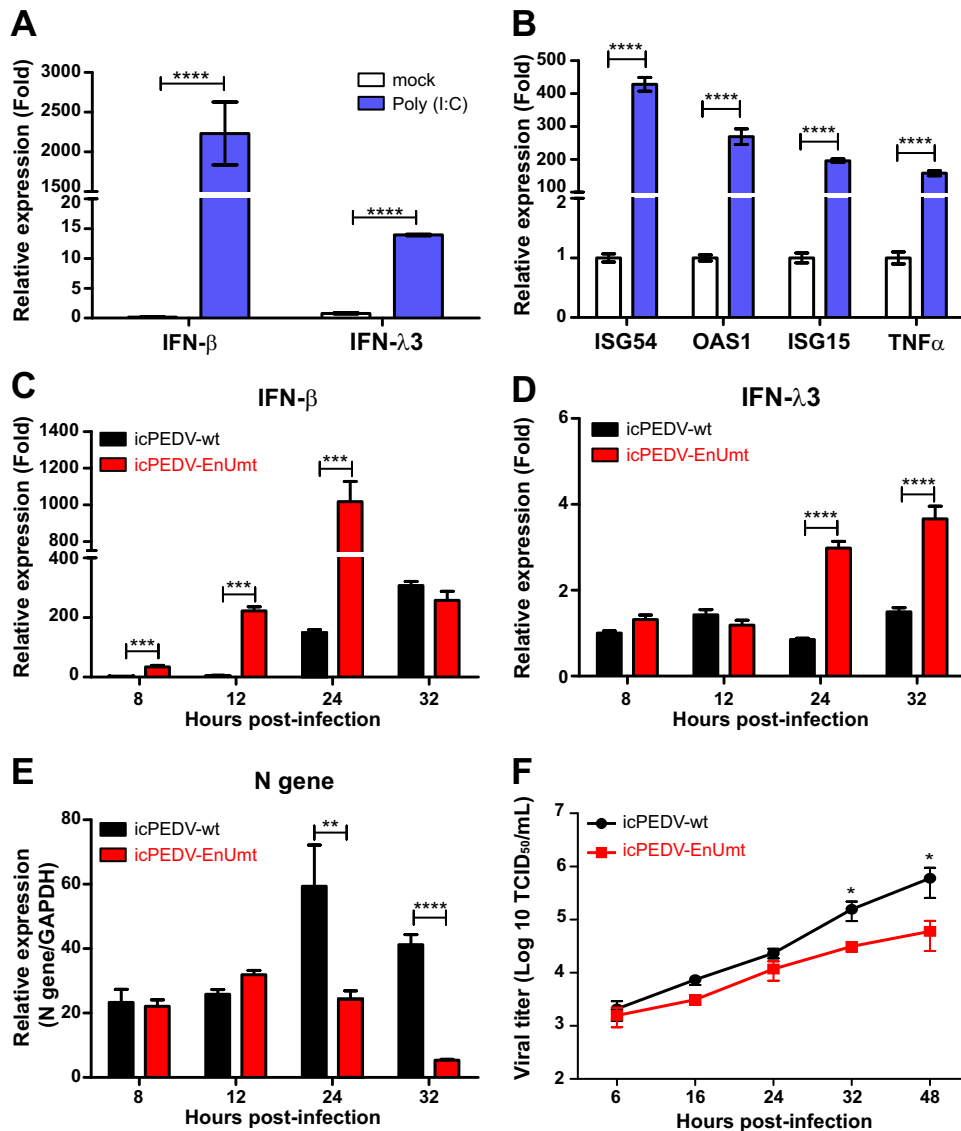


FIG 3 EndoU-deficient PEDV induces early and robust type I and III IFN responses in PK1 cells. (A and B) PK1 cells were transfected with 200 ng poly(I:C) for 24 h. Total RNA was extracted and the relative mRNA levels (compared to levels in mock-treated cells) of (A) IFN-β and IFN-λ3 and (B) ISGs were measured by reverse transcription-quantitative PCR (RT-qPCR). (C to E) PK1 cells were infected with either icPEDV-wt or icPEDV-EnUmt (0.1 TCID₅₀/cell). The relative mRNA levels (comparing to levels in WT-infected cells at 8 h postinfection) of IFN-β (C) and IFN-λ3 (D) were presented as fold changes. The level of N gene (E) relative to GAPDH mRNA were expressed as $2^{-\Delta\Delta C_T} [\Delta C_T = C_{T(\text{gene of interest})} - C_{T(\beta\text{-actin})}]$. (F) PK1 cells were infected with PEDV (0.1 TCID₅₀/cell) and culture supernatant was collected at indicated time points and titrated on Vero cells. The experiment was performed three times and the representative data are shown. Error bars represent mean \pm standard deviation (SD). *, $P < 0.05$; **, $P < 0.01$; ***, $P < 0.001$; ****, $P < 0.0001$.

EnUmt at a dose of 0.1 TCID₅₀ per cell and assessed the mRNA levels of IFN-α, IFN-β and IFN-λ3. As shown in Fig. 5, we observed significantly elevated production of IFN-β mRNA levels, 200- to 500-fold higher than those of mock-infected or icPEDV-wt-infected cells at 6 and 12 hpi, respectively (Fig. 5A). We also detected elevated levels of IFN-α mRNA (Fig. 5B) in cells infected with the icPEDV-EnUmt compared to the levels seen in icPEDV-wt-infected cells. The IFN-λ3 mRNA level was slightly elevated (2-fold) at 24 hpi in icPEDV-EnUmt-infected cells, but there was no statistically significant difference between wild-type (WT)-infected and EndoU mutant-infected PAMs (Fig. 5C). We note that both WT- and EnUmt-infected PAMs exhibited minimal elevation (2-fold) of N gene expression at 24 hpi (Fig. 5D), consistent with very low levels of virus

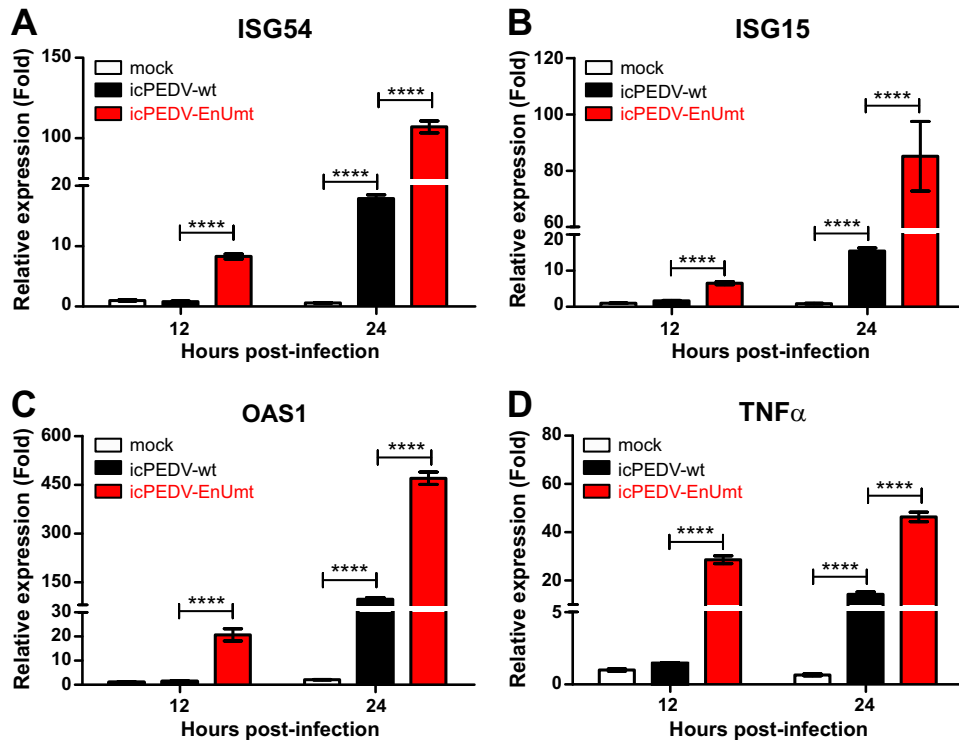


FIG 4 EndoU-deficient PEDV infection induces robust expression of ISGs and proinflammatory cytokines in PK1 cells. PK1 cells were infected with either icPEDV-wt or icPEDV-EnUmt ($0.1 \text{ TCID}_{50}/\text{cell}$), and cells were harvested for total RNA extraction at indicated time points. The relative mRNA levels (comparing to those in mock-infected cells at 12 h postinfection) of ISG54 (A), ISG15 (B), 2'-5'-oligoadenylate synthetase 1 (OAS1) (C), and tumor necrosis factor alpha (TNF- α) (D) were measured using RT-qPCR. The experiment was performed three times, and the representative data are shown. Error bars represent mean \pm SD. ****, $P < 0.0001$.

replication in cultured PAMs (33). We also found that mRNA levels of ISG54 and OAS1 were significantly increased in icPEDV-EnUmt-infected PAMs compared to those in icPEDV-wt-infected PAMs (Fig. 5E and F). These results together indicate that EndoU activity antagonizes the type I IFN response during PEDV infection in primary macrophages.

Evaluating the pathogenesis of PEDV-Colorado parental strain, icPEDV-wt, and icPEDV-EnUmt in piglets. We compared the pathogenicity in piglets of the parental PEDV-Colorado strain with that of the infectious clone viruses. At 7 days of age, eight piglets in a litter were orally inoculated with one of the three viruses (10^5 TCID_{50} per pig). Piglets were monitored daily for clinical symptoms, and daily rectal swabs were collected to evaluate fecal shedding of virus particles. We found that all virus-inoculated piglets manifested with diarrhea and exhibited similar clinical symptoms during the 7-day experimental course, with the icPEDV-EnUmt-infected piglets exhibiting slightly reduced clinical scores at days 3 to 5 (Fig. 6A). Interestingly, although icPEDV-EnUmt-inoculated piglets exhibited a similar disease progression as the WT-infected animals, we found that the icPEDV-EnUmt-infected piglets had significantly reduced viral shedding on days 3 and 6, and trended toward reduced shedding at all time points tested (Fig. 6B). Importantly, there was no mortality in the icPEDV-EnUmt infected piglets, compared to 50% (4/8) and 62.5% (5/8) mortality in the icPEDV-wt and PEDV-Colorado parental strain infected piglets, respectively (Fig. 6C). We performed histopathologic examination of sections of the small intestine in six pigs from the PEDV parental strain-infected group, seven pigs from the icPEDV-EnUmt-infected group and six pigs from the icPEDV-wt-infected group. Lesions consisted of villus atrophy and fusion and accumulation of inflammatory cells within the lamina propria, primarily lymphocytes and plasma

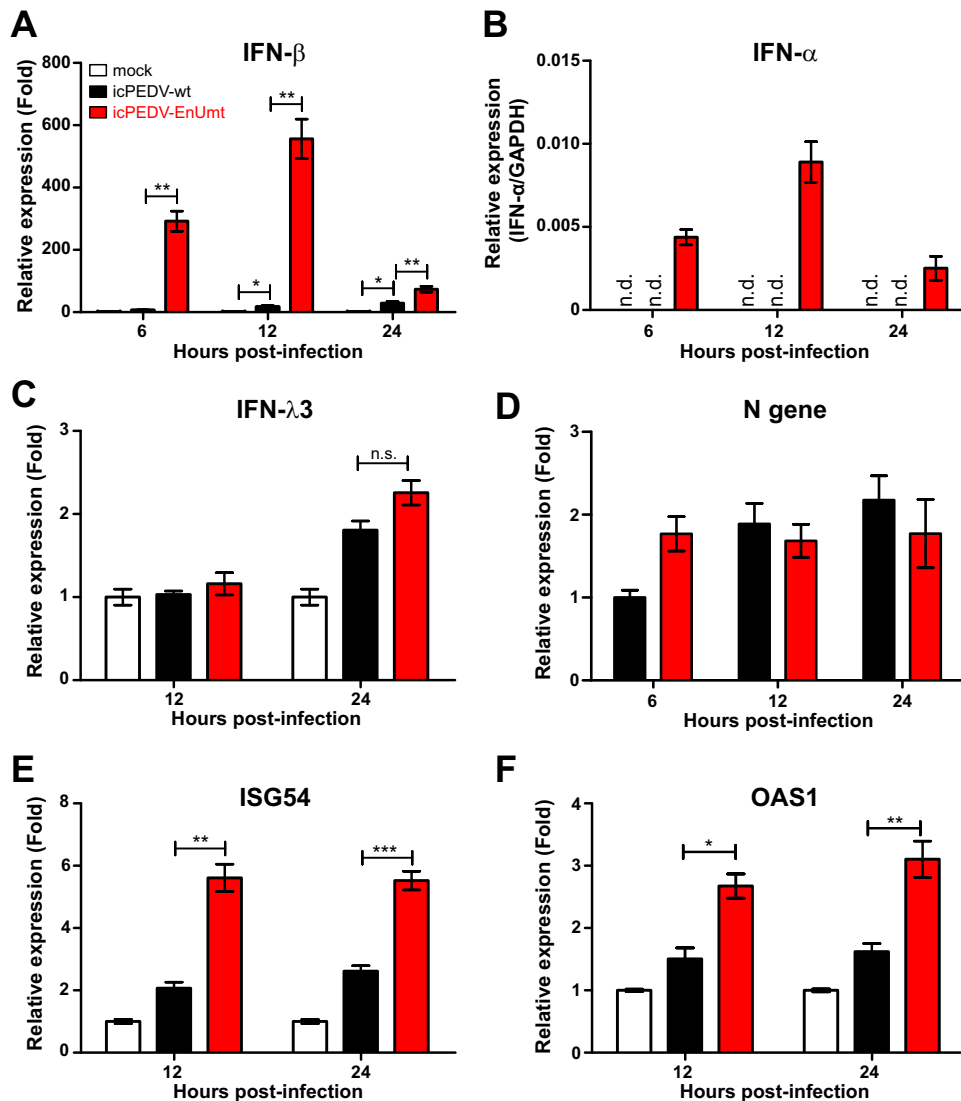


FIG 5 EndoU-deficient PEDV infection induces a robust type I IFN response in primary porcine alveolar macrophages (PAMs). PAMs were infected with either icPEDV-wt or icPEDV-deEndoU (0.1 TCID₅₀/cell), and cells were harvested for total RNA extraction at the indicated time points. The relative mRNA levels (comparing to mock-infected cells) of IFN- β (A), IFN- α (B), IFN- λ 3 (C), ISG54 (E), and OAS1 (F) and the relative N mRNA (D) (comparing to levels in WT-infected cells at 6 h postinfection) were measured using RT-qPCR. The experiment was performed three times, and the representative data are shown. Error bars represent mean \pm SD. n.d., not detectable; n.s., not significant; *, $P < 0.05$; **, $P < 0.01$; ***, $P < 0.001$.

cells, and crypt hyperplasia. Mucosal epithelium in affected sections of intestine was cuboidal to tall columnar, and there was mild exocytosis of inflammatory cells. Lesions were present in one or more intestinal sections from all affected pigs and were most pronounced within sections of jejunum and ileum. We report that lesion severity was not significantly different in affected pigs among the three virus-infected groups; however, individual variation was observed in all groups. Representative images of ileum sections from an age-matched, uninfected piglet and from one piglet per virus-infected group are shown in Fig. 7, upper panel. To determine if the sites of virus replication were similar in all infected animals, we performed immunohistochemistry to detect PEDV nucleocapsid protein. Similarly to previous studies (24–26), viral antigen was detected in epithelial cells, and we found that the sites of replication of the engineered viruses were essentially identical to those found with PEDV-Colorado (Fig. 7, lower panel).

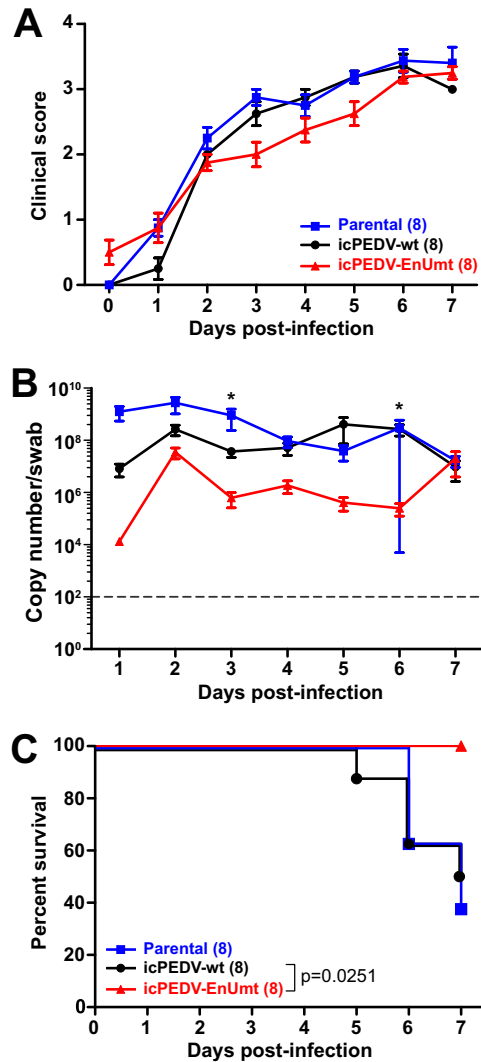


FIG 6 Evaluating the clinical presentation, shedding, and mortality of parental Colorado strain, icPEDV-wt, and icPEDV-EnUmt in neonatal pigs. Seven-day-old piglets were inoculated orally with 10⁵ TCID₅₀ of the indicated strain of PEDV. (A) Clinical symptoms were graded daily for 7 days. (B) Fecal swabs were obtained daily and evaluated for viral RNA by TaqMan RT-qPCR. Error bars represent mean ± SEM; *, *P* < 0.05. The limit of detection for this RT-qPCR assay is indicated by the dotted line. (C) Survival rate was plotted using GraphPad Prism 5, and the *P* value was calculated using the log-rank test. The number (*n*) of animals used in each group is shown in parentheses.

DISCUSSION

Our study reveals that coronaviruses encode a highly conserved enzyme, EndoU, that mitigates type I and type III IFN responses in virus-infected macrophages and epithelial cells. By constructing an infectious clone of the virulent Colorado strain of PEDV and an isogenic strain with a mutation that inactivated EndoU activity, we could directly compare the replication kinetics and innate immune responses of these two viruses in cell culture and in animals. Consistent with previous studies of murine coronavirus (12, 13), we found that both wild-type and the EndoU-mutant PEDV replicate efficiently in interferon deficient Vero cells. However, the loss of EndoU activity correlated with activation of type I (IFN-α/IFN-β) and type III (IFN-λ) IFN responses in macrophages and epithelial cells, and reduced viral titer in PK1 cells. These results are also in line with those of previous reports indicating that replication of SARS-CoV is enhanced in mice lacking the IFN-λ receptor (34, 35) and that PEDV replication can be inhibited by treatment of IFN-λ in epithelial cells (36, 37). Overall, these studies illustrate

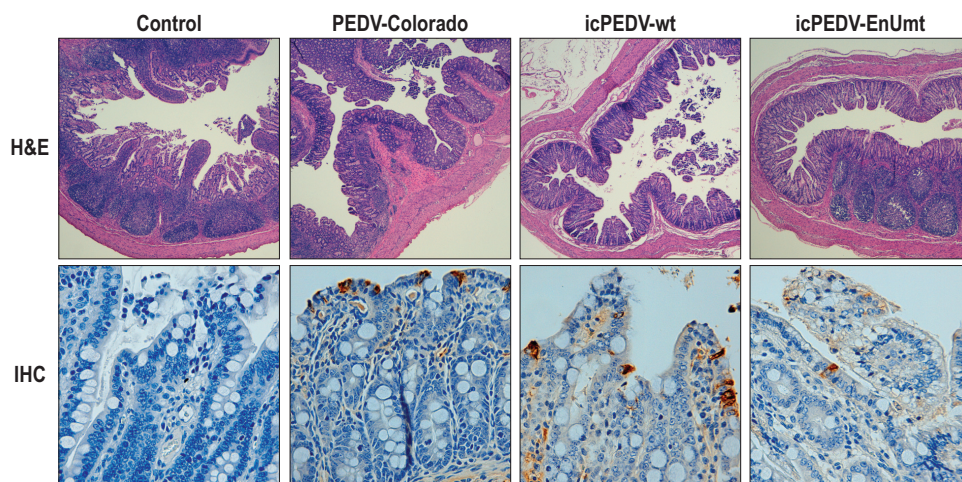


FIG 7 Histology and IHC staining of age-matched uninfected control, PEDV-Colorado, icPEDV-wt-, and icPEDV-EnUmt-infected piglet ileum. Piglets were euthanized at the day 7 time point. Images show representative histological slides of ileum specimens showing H&E staining (upper panel, $\times 4$), and immunohistochemistry (IHC) staining (lower panel, $\times 40$) using mouse anti-PEDV-N antibody.

the critical role of IFNs in controlling enteric pathogens and show that coronaviruses have evolved mechanisms to evade these host innate immune defenses.

Our study illustrates that the innate immune response to PEDV is cell type-specific, with macrophages responding via IFN- α /IFN- β response, whereas the epithelial cell response includes IFN- λ . It is important to note that infection with wild-type PEDV does elicit IFN responses from epithelial cells and macrophages, but the timing of the IFN response is delayed and the magnitude of IFN levels is lower than that in PEDV-EndoU mutant virus infection (Fig. 3). The earlier IFN response elicited by icPEDV-EnUmt infection results in the transcription of a series of ISGs that are known to induce an antiviral state and thereby limit propagation of the invading pathogen. We also report detection of reduced virus shedding and mortality in piglets infected with icPEDV-EnUmt compared to that in piglets infected with the isogenic wild-type strain (Fig. 6B and C). These results suggest that activation of an early innate immune response alters virus replication and pathogenesis, but additional *in vivo* research is needed to fully investigate this issue. For example, the *in vivo* response to CoV infection may differ, depending on the dose of the virus and the age of the animal. It will also be important to evaluate the frequency of reversion of EndoU mutants and to employ strategies to make these viruses recombination resistant (38). It is possible that the pathology we detected at day 7 in the icPEDV-EnUmt-infected animals could be generated by revertant viruses (Fig. 7). Future studies using viruses containing multiple mutations in EndoU, which are thus less likely to revert, should be evaluated at multiple time points to determine the extent of virus replication and the local immune response. For coronaviruses that encode multiple IFN antagonists, it will be interesting to evaluate the role of each antagonist on the type I and type III IFN responses and to determine if inactivating a constellation of antagonists, perhaps both the highly conserved nonstructural protein antagonists and accessory proteins, may be necessary to fully attenuate endemic and emerging strains (29, 39, 40).

Evaluating type III IFN responses in epithelial cells is particularly important for hepatotropic, respiratory, and enterotropic viruses. Previous studies revealed cell type specific differences in the innate immune response and the key role of peroxisomes in activating IFN- λ in response to viral infection. Viral infection recognized by RIG-I/MDA-5 can signal via mitochondrion-associated mitochondrial antiviral-signaling protein (MAVS) to activate interferon regulatory factor 3 (IRF-3) and transcription of IFN- α /IFN- β , or alternatively through peroxisome-associated MAVS to activate IRF-1, resulting in activation of IFN- λ s (41). Hepatitis C virus (HCV) activates both type I and type III IFN

responses (42), but polymorphisms in the IFN- λ gene loci correlate with HCV disease progression and response to treatment (43). This genetic association for controlling HCV replication underscores the importance of the type III IFN response during infection. Similarly, a recent study demonstrates that the IFN- λ response to influenza virus infection provides a “front line” response in the respiratory epithelium to low-dose infection, which facilitates clearance without activation of the type I IFN response (44). Galani and coauthors provide evidence that limiting the viral infection via the type III IFN response mitigates the role of the more proinflammatory type I IFN response, which can be associated with immunopathology. Enterocyte-tropic viruses, such as rotavirus, reovirus, and norovirus, can be limited by type III IFN responses (45–47). Furthermore, IFN- λ receptor knockout mice (*Ifnlr1*^{-/-}) are highly susceptible to these enteric pathogens. Like coronaviruses, some of these viruses encode IFN antagonists to escape the control of the type III IFN response in the gut.

A question that arises from this study is how does EndoU activity antagonize the type I and type III IFN responses? The EndoU crystal structures of SARS-CoV, mouse hepatitis virus, and MERS-CoV have been solved, clearly placing it into a conserved family of endoribonucleases, and mutagenesis studies have validated the role of the conserved histidine residues as essential for catalytic activity (48–50). The nsp15/EndoU protein was shown to localize with other nonstructural proteins and viral RNA in the double membrane vesicles (DMVs) that are thought to protect the viral RNA from recognition by pattern recognition receptors (51–53). Initial reports indicated that EndoU activity was essential for coronavirus replication (16); however, more recent research, including this study of PEDV EndoU, indicate that is not essential for viral replication. Rather, EndoU activity is important for antagonism of the innate immune response in macrophages (12, 13) and, as shown here, in epithelial cells. Our studies using a murine coronavirus indicate that viral dsRNA is detected outside the protection of DMVs in EndoU mutant virus-infected cells, suggested that EndoU activity may play a role in either sequestering or cleaving dsRNA to prevent recognition by host dsRNA sensors such as MDA-5 (13). Further studies are needed to determine the mechanism of CoV EndoU activity in limiting the sensing of viral dsRNA.

The conservation of EndoU across the entire family of the *Coronaviridae*, including related arteriviruses, such as porcine respiratory and reproductive syndrome virus (PRRSV), and emerging coronaviruses, such as swine acute diarrhea syndrome CoV (SADS-CoV) is consistent with a required role for this enzymatic activity. Mutagenesis studies of the arterivirus EndoU revealed pleiotropic effects on replication; however, these mutant viruses were evaluated in BHK-21 cells, which are defective in IFN production (54, 55). Further studies are needed to determine if arterivirus EndoU activity is important for antagonizing type I and type III IFN responses. Regarding SADS-CoV, this virus recently emerged from bats into the swine population in China, causing fatal disease in over 23,000 piglets on four farms (56–58). There are no vaccines currently available to protect from this infection. Identifying the key virulence factors for this emerging virus is essential for designing effective live-attenuated virus vaccines.

This study provides evidence of a role for PEDV EndoU activity in antagonizing both type I and type III IFN responses in macrophages and epithelial cells and documents for the first time that inactivating EndoU activity modulates the virulence of PEDV infection in piglets.

MATERIALS AND METHODS

Cells and virus. Porcine kidney epithelial cells, LLC-PK1 (ATCC CL101), termed PK1 cells, were purchased from the ATCC and grown in growth medium containing modified Eagle medium (MEM) (catalog no. 10010CV; Corning) supplemented with heat-inactivated 5% fetal calf serum (FCS) (Atlanta Biological) and 1% penicillin/streptomycin (pen/strep; HyClone). Vero cells (USDA Animal and Plant Health Inspection Agency, National Veterinary Services Laboratory [APHIS-NVSL]) were grown in growth media containing MEM (catalog no. 41500-018; Gibco) supplemented with 10% FCS, 0.5% lactalbumin enzymatic hydrolysate (catalog no. 68458-87-7; Sigma), and 1% pen/strep. Porcine alveolar macrophages (PAMs) were isolated from healthy young pigs by lung lavage and maintained in RPMI 1640 medium (catalog no. 10043CVR; Corning) supplemented with 10% FCS and 1% pen/strep. The Colorado strain of PEDV (USA/Colorado/2013; GenBank accession number [KF272920](https://www.ncbi.nlm.nih.gov/nuccore/KF272920)) was obtained from APHIS-NVSL and

passed four times in our laboratory. To make a large stock, PEDV was propagated once more in Vero cells with maintenance media containing FCS-free growth media, 0.15% Bacto tryptose phosphate broth (29.5 g/liter, catalog no. 260300, Bectin Dickinson), and 2 $\mu\text{g}/\text{ml}$ 6-(1-tosylamido-2-phenyl) ethyl chloromethyl ketone (TPCK)-treated trypsin (catalog no. LS003750; Worthington Biochemicals). The culture medium of infected cells was harvested when $\sim 90\%$ cells showed cytopathic effect (CPE), titrated on Vero cell monolayers, and stored at -80°C .

Construction of an infectious clone of PEDV-Colorado strain. A previously published approach for generation of a CoV reverse genetics system (27) was used to assemble a full-length PEDV cDNA clone. Briefly, the genomic sequence of the Colorado strain was divided into five fragments (PEDV-A to PEDV-E) flanked with unique class II restriction sites that leave nonpalindromic overhangs. These fragments were obtained by PCR amplification from three large synthetic DNAs (GenScript) based on the genomic sequence of the fourth passage of PEDV-Colorado strain in Vero cells and sequenced by the Iowa State Veterinary Diagnostic Laboratory. In the PEDV-A fragment, a promoter sequence of T7 RNA polymerase was added upstream from the sequence of the PEDV 5' untranslated region (UTR). In the E fragment, two synonymous mutations (A23309G and A23312G) were introduced to disrupt a stretch of six A nucleotides, which might interfere with *in vitro* RNA transcription reactions. Additionally, three nucleotides (GGC) were inserted into the E fragment at nucleotide site 22030 of the PEDV genome. This insertion resulted in a replacement of aspartate 466 residue with a glycine and a histidine (D466GH) in the spike protein, which was shown to facilitate the cell adaptation of PEDV and recovery of infectious clone virus (30). The E fragment also contains a poly(A) tail (23 As) at the end of the viral genomic sequence. All five fragments were cloned into the pCR-XL-TOPO vector, amplified in TOP10 bacterial cells, and verified by Sanger sequencing. A large quantity of each PEDV fragment was obtained by digesting the recombinant plasmid DNA using restriction sites designated in Fig. 1, separating the DNA fragments on a 1% low-melt agarose gel (catalog no. 50111; Lonza), excising the DNA fragment from the gel, and purifying the DNA fragment using a Wizard SV gel extraction kit (catalog no. A9282; Promega). All five PEDV fragments were mixed and ligated overnight at 16°C using T4 DNA ligase (catalog no. M0202L; New England Biolabs). Ligated fragments were extracted with phenol-chloroform and used as a template for *in vitro* T7 RNA transcription as instructed in the mMessage mMachine T7 transcription kit (catalog no. AM1344, Life Technologies). In addition, the PEDV nucleocapsid (N) gene was cloned into the pcDNA3.1 vector containing a T7 promoter sequence. N gene transcripts were generated from the digested N gene fragment using recommended conditions (mMessage mMachine T7 transcription kit). Viral RNA and N gene transcripts were mixed with 800 μl of Vero cells (1×10^7 cells/ml) in Opti-MEM (catalog no. 11058021; Gibco) and then added to an electroporation cuvette. Three pulses of 450 V at 50 μF were used to electroporate RNA into cells with a Gene Pulser II electroporator (Bio-Rad). The cells were recovered in the cuvette for 10 min at room temperature and then were cultured in a 75-cm² flask in growth medium at 37°C and 5% CO₂. The growth medium was replaced with FCS-free maintenance medium containing 2 $\mu\text{g}/\text{ml}$ TPCK-treated trypsin 16 h postelectroporation. Cells were maintained until over 90% of the cell monolayer showed syncytia-like CPE, and then the supernatant was harvested and stored at -80°C . To generate an EndoU-deficient PEDV, two nucleotides were mutated (C19390G and A19391C) in fragment D to produce a histidine-to-alanine substitution in nsp15. The mutated D fragment was combined with the other fragments for generation of an EndoU-deficient PEDV. Aliquots of both recombinant viral stocks were sent to the Iowa State Veterinary Diagnostic Laboratory for full genome sequencing. Except for the mutations described previously, no additional changes were detected.

Growth kinetics and titration. In a 24-well (1.5×10^5 cells/well) plate, Vero cells were infected with PEDV at a dose of 0.1 TCID₅₀ per cell in the presence of 2 $\mu\text{g}/\text{ml}$ TPCK-treated trypsin. After two hours incubation, the inoculum was removed and replaced with Vero cell maintenance medium. Cell culture supernatant was collected at the indicated time points after infection and subjected to titration using a standard TCID₅₀ assay. Briefly, Vero cells seeded in a 96-well plate (4×10^4 cells/well) were washed three times with phosphate-buffered saline (PBS) and then incubated with serially 10-fold diluted supernatant from infected cells. The number of wells with visible CPE were counted ~ 3 to 4 days postinfection. The TCID₅₀ value was calculated using the Reed-Muench method (59).

Immunofluorescence assay. In a 96-well plate, Vero cells were infected with PEDV at a dose of 0.1 TCID₅₀ per cell in the presence of 2 $\mu\text{g}/\text{ml}$ TPCK-treated trypsin. At 16 h postinfection, cells were washed once with PBS and fixed with cold methanol/acetone (50%/50%, vol/vol) for 15 min at -20°C . Fixed cells were then blocked with PBS containing 5% FCS for 30 min at 37°C and stained with FITC-labeled anti-N protein monoclonal antibody (mAb SD6-29; courtesy of Eric A. Nelson, South Dakota State University) for 1 h at 37°C . Subsequently, cells were washed three times with PBS before examination using a fluorescence microscope.

Evaluating transcript levels from cultured cells. To measure mRNA levels from cells, 3×10^5 PK1 cells or 6×10^5 PAMs per well were plated in a 12-well plate 16 h prior to infection. Cells were washed twice with PBS and infected with the indicated virus at a dose of 0.1 TCID₅₀ per cell in the presence of 5 $\mu\text{g}/\text{ml}$ trypsin (catalog no. 59427C; Sigma). Cells were harvested at different time points using RLT buffer provided by the RNeasy minikit (catalog no. 74104; Qiagen), and total RNA was extracted as instructed by the manufacturer's protocol. A 500-ng sample of RNA was used for cDNA synthesis using the RT2 HT first strand kit (catalog no. 330411; Qiagen). Quantitative PCR (qPCR) was performed using RT2 SYBR green qPCR mix (catalog no. 330502; Qiagen) in the Bio-Rad CFX96 system. The thermocycler was set as follows: one step at 95°C (10 min), 40 cycles of 95°C (15 s), 55°C (1 min) and plate read, one step at 95°C (10 s), and a melt curve from 65°C to 95°C in increments of $0.5^\circ\text{C}/0.05$ s. Samples were assayed in triplicate and data are representative of three independent experiments. The levels of mRNA

TABLE 1 qPCR primer and probe sequences used in this study

Method	Target	Forward (5'→3')	Reverse (5'→3')
SYBR green	Porcine IFN- α	CCTGGCACAAATGAGGAGAA	GCCTTCTGGACCTGGTTG
	Porcine IFN- β	AGCAGATCTTCGGCATTCTC	GTCATCCATCTGCCCATCAA
	Porcine IFN- λ 3	GTTC AAGTCTCTGTCCCCAC	GCTGCAGTCCAGTCCTC
	Porcine GAPDH	ACCTCCACTACATGGTCTACA	ATGACAAGCTTCCCGTTCTC
	PEDV N gene	CACTAACCTGGGTGTCAGAAA	CGTGAAGTAGGAGGTGTGTTAG
TaqMan	PEDV N gene	GAATTCCTCAAGGGCGAAAAT	TTTTGCACAAATTCGCGATCT
	N gene probe	FAM-CGTAGCAGCTTGCTTCGGACCCA-BHQ ^a	

^aFAM, 6-carboxyfluorescein; BHQ, black hole quencher.

were relative to β -actin mRNA and were expressed as $2^{-\Delta C_T}$ [$\Delta C_T = C_{T(\text{gene of interest})} - C_{T(\text{GAPDH})}$], where C_T indicates cycle threshold. PCR primers used in this study are listed in Table 1.

Animal study. Three pregnant sows free of clinical disease were purchased from a PEDV-negative herd and transported to NADC about 4 weeks prior to farrowing. They were housed as a group according to National Animal Disease Center (NADC) Institutional Animal Care and Use Guidelines and randomly assigned to treatment groups. At 7 to 10 days prior to farrowing, each sow was placed in a farrowing crate in an isolation room and allowed to farrow naturally. At 7 days of age, 8 piglets in each litter were orally inoculated with the indicated virus in a 2-ml volume containing 1×10^5 TCID₅₀/ml of virus. Clinical diarrhea signs were recorded daily and graded based on severity using the following criteria: 0 = healthy, normal feces; 1 = soft stool; 2 = semiliquid stool; 3 = projectile liquid feces; and 4 = voluminous watery diarrhea (60). Rectal swabs were collected daily using a sterile polyester-tipped applicator immersed in a 5-ml polystyrene round-bottom tube filled with 2 ml of MEM. All samples were frozen at -80°C until future use.

Quantifying viral RNA from fecal samples. The quantification of viral RNAs in fecal samples has been previously described (61). Briefly, each sample was thawed, vortexed for ~ 10 s, and then centrifuged to clarify. RNA extraction was performed with 200 μl of the supernatant from each rectal swab by using a MagMax pathogen RNA/DNA kit (catalog no. 4462359; Applied Biosystems) in a MagMax Express (Applied Biosystems) instrument according to the manufacturer's feces total nucleic acid purification protocol. Viral RNA was eluted into 90 μl of buffer. PEDV N gene reverse transcription-PCR (RT-PCR) was performed on nucleic acid extracts using Ambion Path ID multiplex one-step RT-PCR master mix (catalog no. 4442137; Applied Biosystems) according to the manufacturer's recommendations for the 7500 fast real-time PCR system (Applied Biosystems). The reverse transcription was performed at 45°C for 10 min and reverse transcriptase denaturation at 95°C for 10 min, followed by 40 cycles of 95°C for 15 sec and 60°C for 45 sec, during which fluorescence was collected. Primers and probe targeted conserved regions (nucleotides 941 to 1028) of the PEDV N gene with modifications specific to the PEDV strain USA/Colorado/2013 (GenBank accession number [KF272920](https://www.ncbi.nlm.nih.gov/nuclom/KF272920)). The sequences of probe and primers are listed in Table 1.

H&E staining and immunohistochemistry. Tissues were fixed in neutral buffered formalin and then routinely processed and embedded in paraffin. Five-micron-thick sections were cut and routinely stained with hematoxylin and eosin (H&E) stain utilizing a Tissue-Tek automated slide stainer (Sakura Finetek USA, Torrance, CA). A veterinary pathologist who was blind to the treatment groups evaluated sections of small intestine by light microscopy to identify location and subjectively assess villus atrophy and crypt hyperplasia.

Formalin-fixed, paraffin-embedded intestinal tissue sections were mounted on positively charged glass slides and oven dried for 60 min at 60°C . Slides were deparaffinized using a preprogrammed protocol on a Tissue-Tek Prisma automated slide stainer (Sakura Finetek USA, Torrance, CA). Deparaffinized slides were then rinsed three times in deionized water, followed by soaking in Tris buffer saline with Tween 20 for 5 min. Slides were placed in a Dako autostainer (Agilent, Santa Clara, CA) and run through a preprogrammed immunohistochemistry (IHC) protocol. The IHC protocol utilizes Protease XIV (Millipore Sigma, St. Louis, MO) for antigen retrieval, murine monoclonal antibody SD6-29 specific for the nucleocapsid of PEDV (62) at 1:1,000 dilution, Dako Envision+HRP (Agilent, Santa Clara, CA), and DAB substrate chromogen (Agilent, Santa Clara, CA). The slides were then counterstained in hematoxylin and cover slipped. The same veterinary pathologist who evaluated the H&E stained intestinal sections also evaluated the IHC slides.

ACKNOWLEDGMENTS

We thank Jason Huegel, Keiko Sampson, and Justin Miller for providing animal care, Sarah Anderson and Deb Adolphson for technical assistance (animal handling, RT-qPCR), and Robert C. Mettelman and Matthew Hackbart for comments and suggestions.

This work was funded by the USDA-Loyola University Chicago cooperative agreement no. 59-5030-8-003B (to S.C.B.), NIH AI085089 (to S.C.B.) and USDA ARS CRIS project 5030-32000-108-00D (to K.S.F.).

REFERENCES

1. Chan YK, Gack MU. 2016. Viral evasion of intracellular DNA and RNA sensing. *Nat Rev Microbiol* 14:360–373. <https://doi.org/10.1038/nrmicro.2016.45>.
2. García-Sastre A. 2017. Ten strategies of interferon evasion by viruses. *Cell Host Microbe* 22:176–184. <https://doi.org/10.1016/j.chom.2017.07.012>.
3. Lee S, Baldrige MT. 2017. Interferon-lambda: a potent regulator of intestinal viral infections. *Front Immunol* 8:749. <https://doi.org/10.3389/fimmu.2017.00749>.
4. Lazear HM, Nice TJ, Diamond MS. 2015. Interferon-λ: immune functions at barrier surfaces and beyond. *Immunity* 43:15–28. <https://doi.org/10.1016/j.immuni.2015.07.001>.
5. Wack A, Terczyńska-Dyla E, Hartmann R. 2015. Guarding the frontiers: the biology of type III interferons. *Nat Immunol* 16:802–809. <https://doi.org/10.1038/ni.3212>.
6. de Wit E, van Doremalen N, Falzarano D, Munster VJ. 2016. SARS and MERS: recent insights into emerging coronaviruses. *Nat Rev Microbiol* 14:523–534. <https://doi.org/10.1038/nrmicro.2016.81>.
7. Menachery VD, Graham RL, Baric RS. 2017. Jumping species—a mechanism for coronavirus persistence and survival. *Curr Opin Virol* 23:1–7. <https://doi.org/10.1016/j.coviro.2017.01.002>.
8. Channappanavar R, Fehr AR, Vijay R, Mack M, Zhao J, Meyerholz DK, Perlman S. 2016. Dysregulated type I interferon and inflammatory monocyte-macrophage responses cause lethal pneumonia in SARS-CoV-infected mice. *Cell Host Microbe* 19:181–193. <https://doi.org/10.1016/j.chom.2016.01.007>.
9. Egli A, Santer DM, O’Shea D, Tyrrell DL, Houghton M. 2014. The impact of the interferon-lambda family on the innate and adaptive immune response to viral infections. *Emerg Microbes Infect* 3:1. <https://doi.org/10.1038/emi.2014.51>.
10. Kutenko SV, Durbin JE. 2017. Contribution of type III interferons to antiviral immunity: location, location, location. *J Biol Chem* 292:7295–7303. <https://doi.org/10.1074/jbc.R117.777102>.
11. Kindler E, Thiel V. 2014. To sense or not to sense viral RNA—essentials of coronavirus innate immune evasion. *Curr Opin Microbiol* 20:69–75. <https://doi.org/10.1016/j.mib.2014.05.005>.
12. Kindler E, Gil-Cruz C, Spanier J, Li Y, Wilhelm J, Rabouw HH, Züst R, Hwang M, V’kovski P, Stalder H, Marti S, Habjan M, Cervantes-Barragan L, Elliot R, Karl N, Gaughan C, van Kuppeveld FJM, Silverman RH, Keller M, Ludewig B, Bergmann CC, Ziebuhr J, Weiss SR, Kalinke U, Thiel V. 2017. Early endonuclease-mediated evasion of RNA sensing ensures efficient coronavirus replication. *PLoS Pathog* 13:e1006195. <https://doi.org/10.1371/journal.ppat.1006195>.
13. Deng X, Hackbart M, Mettelman RC, O’Brien A, Mielech AM, Yi G, Kao CC, Baker SC. 2017. Coronavirus nonstructural protein 15 mediates evasion of dsRNA sensors and limits apoptosis in macrophages. *Proc Natl Acad Sci U S A* 114:E4251–E4260. <https://doi.org/10.1073/pnas.1618310114>.
14. Deng X, Baker SC. 2018. An “Old” protein with a new story: coronavirus endoribonuclease is important for evading host antiviral defenses. *Virology* 517:157–163. <https://doi.org/10.1016/j.virol.2017.12.024>.
15. Bhardwaj K, Guarino L, Kao CC. 2004. The severe acute respiratory syndrome coronavirus Nsp15 protein is an endoribonuclease that prefers manganese as a cofactor. *J Virol* 78:12218–12224. <https://doi.org/10.1128/JVI.78.22.12218-12224.2004>.
16. Ivanov KA, Hertzog T, Rozanov M, Bayer S, Thiel V, Gorbalenya AEA, Ziebuhr J. 2004. Major genetic marker of nidoviruses encodes a replicative endoribonuclease. *Proc Natl Acad Sci U S A* 101:12694–12699. <https://doi.org/10.1073/pnas.0403127101>.
17. Kang H, Bhardwaj K, Li Y, Palaninathan S, Sacchettini J, Guarino L, Leibowitz JL, Cheng Kao C, Kao CC. 2007. Biochemical and genetic analyses of murine hepatitis virus Nsp15 endoribonuclease. *J Virol* 81:13587–13597. <https://doi.org/10.1128/JVI.00547-07>.
18. Cima G. 2013. Viral disease affects U.S. pigs: porcine epidemic diarrhea found in at least 11 states. *J Am Vet Med Assoc* 243:30–31.
19. Huang Y-W, Dickerman AW, Piñeyro P, Li L, Fang L, Kiehne R, Opriessnig T, Meng X-J. 2013. Origin, evolution, and genotyping of emergent porcine epidemic diarrhea virus strains in the United States. *mBio* 4:e00737–e00713. <https://doi.org/10.1128/mBio.00737-13>.
20. Stevenson GW, Hoang H, Schwartz KJ, Burrough ER, Sun D, Madson D, Cooper VL, Pillatzki A, Gauger P, Schmitt BJ, Koster LG, Killian ML, Yoon KJ. 2013. Emergence of *Porcine epidemic diarrhea virus* in the United States: clinical signs, lesions, and viral genomic sequences. *J Vet Diagn Invest* 25:649–654. <https://doi.org/10.1177/1040638713501675>.
21. Crawford K, Lager KM, Kulshreshtha V, Miller LC, Faaberg KS. 2016. Status of vaccines for porcine epidemic diarrhea virus in the United States and Canada. *Virus Res* 226:108–116. <https://doi.org/10.1016/j.virusres.2016.08.005>.
22. Langel SN, Paim FC, Lager KM, Vlasova AN, Saif LJ. 2016. Lactogenic immunity and vaccines for porcine epidemic diarrhea virus (PEDV): Historical and current concepts. *Virus Res* 226:93–107. <https://doi.org/10.1016/j.virusres.2016.05.016>.
23. Jung K, Saif LJ. 2015. Porcine epidemic diarrhea virus infection: Etiology, epidemiology, pathogenesis and immunoprophylaxis. *Vet J* 204:134–143. <https://doi.org/10.1016/j.tvjl.2015.02.017>.
24. Jung K, Wang Q, Scheuer KA, Lu Z, Zhang Y, Saif LJ. 2014. Pathology of US porcine epidemic diarrhea virus strain PC21A in gnotobiotic pigs. *Emerg Infect Dis* 20:668–671. <https://doi.org/10.3201/eid2004.131685>.
25. Madson DM, Arruda PHE, Magstadt DR, Burrough ER, Hoang H, Sun D, Bower LP, Bhandari M, Gauger PC, Stevenson GW, Wilberts BL, Wang C, Zhang J, Yoon KJ. 2016. Characterization of porcine epidemic diarrhea virus isolate US/Iowa/18984/2013 infection in 1-day-old cesarean-derived colostrum-deprived piglets. *Vet Pathol* 53:44–52. <https://doi.org/10.1177/0300985815591080>.
26. Niederwerder MC, Nietfeld JC, Bai J, Peddireddi L, Breazeale B, Anderson J, Kerrigan MA, An B, Oberst RD, Crawford K, Lager KM, Madson DM, Rowland RRR, Anderson GA, Hesse RA. 2016. Tissue localization, shedding, virus carriage, antibody response, and aerosol transmission of *Porcine epidemic diarrhea virus* following inoculation of 4-week-old feeder pigs. *J Vet Diagn Invest* 28:671–678. <https://doi.org/10.1177/1040638716663251>.
27. Yount B, Denison MR, Weiss SR, Ralph S, Baric RS. 2002. Systematic assembly of a full-length infectious cDNA of mouse hepatitis virus strain A59. *J Virol* 76:11065–11078. <https://doi.org/10.1128/JVI.76.21.11065-11078.2002>.
28. Marthaler D, Jiang Y, Otterson T, Goyal S, Rossow K, Collins J. 2013. Complete genome sequence of porcine epidemic diarrhea virus strain USA/Colorado/2013 from the United States. *Genome Announc* 1:e00555–e00513.
29. Beall A, Yount B, Lin C-M, Hou Y, Wang Q, Saif L, Baric RS. 2016. Characterization of a pathogenic full-length cDNA clone and transmission model for porcine epidemic diarrhea virus strain. *mBio* 7:1–10.
30. Hou Y, Lin C-M, Yokoyama M, Yount BL, Marthaler D, Douglas AL, Ghimire S, Qin Y, Baric RS, Saif LJ, Wang Q. 2017. Deletion of a 197-amino-acid region in the N-terminal domain of spike protein attenuates porcine epidemic diarrhea virus in piglets. *J Virol* 91:e00227–e00217.
31. Hu H, Jung K, Vlasova AN, Chepngeno J, Lu Z, Wang Q, Saif LJ. 2015. Isolation and characterization of porcine deltacoronavirus from pigs with diarrhea in the United States. *J Clin Microbiol* 53:1537–1548. <https://doi.org/10.1128/JCM.00031-15>.
32. Zhang Q, Ma J, Yoo D. 2017. Inhibition of NF-κB activity by the porcine epidemic diarrhea virus nonstructural protein 1 for innate immune evasion. *Virology* 510:111–126. <https://doi.org/10.1016/j.virol.2017.07.009>.
33. Park JE, Shin HJ. 2014. Porcine epidemic diarrhea virus infects and replicates in porcine alveolar macrophages. *Virus Res* 191:143–152. <https://doi.org/10.1016/j.virusres.2014.07.038>.
34. Mordstein M, Neugebauer E, Ditt V, Jessen B, Rieger T, Falcone V, Sorgeloos F, Ehl S, Mayer D, Kochs G, Schwemmler M, Günther S, Drosten C, Michiels P, Staeheli P. 2010. Lambda interferon renders epithelial cells of the respiratory and gastrointestinal tracts resistant to viral infections. *J Virol* 84:5670–5677. <https://doi.org/10.1128/JVI.00272-10>.
35. Mahlakoiv T, Ritz D, Mordstein M, DeDiego ML, Enjuanes L, Muller MA, Drosten C, Staeheli P. 2012. Combined action of type I and type III interferon restricts initial replication of severe acute respiratory syndrome coronavirus in the lung but fails to inhibit systemic virus spread. *J Gen Virol* 93:2601–2605. <https://doi.org/10.1099/vir.0.046284-0>.
36. Li L, Fu F, Xue M, Chen W, Liu J, Shi H, Chen J, Bu Z, Feng L, Liu P. 2017. IFN-lambda preferably inhibits PEDV infection of porcine intestinal epithelial cells compared with IFN-alpha. *Antiviral Res* 140:76–82. <https://doi.org/10.1016/j.antiviral.2017.01.012>.
37. Zhang Q, Ke H, Blikslager A, Fujita T, Yoo D. 2018. Type III interferon restriction by porcine epidemic diarrhea virus and the role of viral protein nsp1 in IRF1 signaling. *J Virol* 92:e01677–e01617.

38. Yount B, Roberts RS, Lindesmith L, Baric RS. 2006. Rewiring the severe acute respiratory syndrome coronavirus (SARS-CoV) transcription circuit: engineering a recombination-resistant genome. *Proc Natl Acad Sci U S A* 103:12546–12551. <https://doi.org/10.1073/pnas.0605438103>.
39. Menachery VD, Gralinski LE, Mitchell HD, Dinno KH, Leist SR, Yount BL, McAnarney ET, Graham RL, Waters KM, Baric RS. 2018. Combination attenuation offers strategy for live-attenuated coronavirus vaccines. *J Virol* 92:e00710-18.
40. Zhang Q, Shi K, Yoo D. 2016. Suppression of type I interferon production by porcine epidemic diarrhea virus and degradation of CREB-binding protein by nsp1. *Virology* 489:252–268. <https://doi.org/10.1016/j.virol.2015.12.010>.
41. Odendall C, Dixit E, Stavru F, Bierre H, Franz KM, Durbin AF, Boulant S, Gehrke L, Cossart P, Kagan JC. 2014. Diverse intracellular pathogens activate type III interferon expression from peroxisomes. *Nat Immunol* 15:717–726. <https://doi.org/10.1038/ni.2915>.
42. Bender S, Reuter A, Eberle F, Einhorn E, Binder M, Bartenschlager R. 2015. Activation of type I and III interferon response by mitochondrial and peroxisomal MAVS and inhibition by hepatitis C virus. *PLoS Pathog* 11:e1005264. <https://doi.org/10.1371/journal.ppat.1005264>.
43. Griffiths SJ, Dunnigan CM, Russell CD, Haas JG. 2015. The role of interferon- λ locus polymorphisms in hepatitis C and other infectious diseases. *J Innate Immun* 7:231–242. <https://doi.org/10.1159/000369902>.
44. Galani IE, Triantafyllia V, Eleminiadou E-E, Koltsida O, Stavropoulos A, Manioudaki M, Thanos D, Doyle SE, Kotenko SV, Thanopoulou K, Andreakos E. 2017. Interferon- λ mediates non-redundant front-line antiviral protection against influenza virus infection without compromising host fitness. *Immunity* 46:875–890.e6. <https://doi.org/10.1016/j.immuni.2017.04.025>.
45. Mählaköiv T, Hernandez P, Gronke K, Diefenbach A, Staeheli P. 2015. Leukocyte-derived IFN- α/β and epithelial IFN- λ constitute a compartmentalized mucosal defense system that restricts enteric virus infections. *PLoS Pathog* 11:e1004782. <https://doi.org/10.1371/journal.ppat.1004782>.
46. Lee S, Wilen CB, Orvedahl A, McCune BT, Kim K-W, Orchard RC, Peterson ST, Nice TJ, Baldrige MT, Virgin HW. 2017. Norovirus cell tropism is determined by combinatorial action of a viral non-structural protein and host cytokine. *Cell Host Microbe* 22:449–459.e4. <https://doi.org/10.1016/j.chom.2017.08.021>.
47. Baldrige MT, Lee S, Brown JJ, McAllister N, Urbanek K, Dermody TS, Nice TJ, Virgin HW. 2017. Expression of *Ifnl1* on intestinal epithelial cells is critical to the antiviral effects of interferon lambda against norovirus and reovirus. *J Virol* 91:e02079-16. <https://doi.org/10.1128/JVI.02079-16>.
48. Ricagno S, Egloff M-PM-P, Ulferts R, Coutard B, Nurizzo D, Campanacci V, Cambillau C, Ziebuhr J, Canard B. 2006. Crystal structure and mechanistic determinants of SARS coronavirus nonstructural protein 15 define an endoribonuclease family. *Proc Natl Acad Sci U S A* 103:11892–11897. <https://doi.org/10.1073/pnas.0601708103>.
49. Xu X, Zhai Y, Sun F, Lou Z, Su D, Xu Y, Zhang R, Joachimiak A, Zhang XC, Bartlam M, Rao Z. 2006. New antiviral target revealed by the hexameric structure of mouse hepatitis virus nonstructural protein nsp15. *J Virol* 80:7909–7917. <https://doi.org/10.1128/JVI.00525-06>.
50. Zhang L, Li L, Yan L, Ming Z, Jia Z, Lou Z, Rao Z. 2018. Structural and biochemical characterization of endoribonuclease Nsp15 encoded by Middle East respiratory syndrome coronavirus. *J Virol* 92:e00893–e00818.
51. Shi ST, Schiller JJ, Kanjanahaluethai A, Baker SC, Oh JW, Lai MM. 1999. Colocalization and membrane association of murine hepatitis virus gene 1 products and *de novo*-synthesized viral RNA in infected cells. *J Virol* 73:5957–5969.
52. Athmer J, Fehr AR, Grunewald M, Smith EC, Denison MR, Perlman S. 2017. *In situ* tagged nsp15 reveals interactions with coronavirus replication/transcription complex associated proteins. *mBio* 8:e02320-16. <https://doi.org/10.1128/mBio.02320-16>.
53. Knoops K, Kikkert M, Worm SHE, van den Zeehoven-Dobbe JC, van der Meer Y, Koster AJ, Mommaas AM, Snijder EJ. 2008. SARS-coronavirus replication is supported by a reticulovesicular network of modified endoplasmic reticulum. *PLoS Biol* 6:e226. <https://doi.org/10.1371/journal.pbio.0060226>.
54. Posthuma CC, Nedialkova DD, Zevenhoven-Dobbe JC, Blokhuis JH, Gorbalenya AE, Snijder EJ. 2006. Site-directed mutagenesis of the nidovirus replicative endoribonuclease NendoU exerts pleiotropic effects on the arterivirus life cycle. *J Virol* 80:1653–1661. <https://doi.org/10.1128/JVI.80.4.1653-1661.2006>.
55. Sun Y, Ke H, Han M, Chen N, Fang W, Yoo D. 2016. Nonstructural protein 11 of porcine reproductive and respiratory syndrome virus suppresses both MAVS and RIG-I expression as one of the mechanisms to antagonize type I interferon production. *PLoS One* 11:e0168314. <https://doi.org/10.1371/journal.pone.0168314>.
56. Gong L, Li J, Zhou Q, Xu Z, Chen L, Zhang Y, Xue C, Wen Z, Cao Y. 2017. A new bat-HKU2-like coronavirus in swine, China, 2017. *Emerg Infect Dis* 23:1607–1609. <https://doi.org/10.3201/eid2309.170915>.
57. Pan Y, Tian X, Qin P, Wang B, Zhao P, Yang Y-L, Wang L, Wang D, Song Y, Zhang X, Huang Y-W. 2017. Discovery of a novel swine enteric alphacoronavirus (SeACoV) in southern China. *Vet Microbiol* 211:15–21. <https://doi.org/10.1016/j.vetmic.2017.09.020>.
58. Zhou P, Fan H, Lan T, Yang X-L, Shi W-F, Zhang W, Zhu Y, Zhang Y-W, Xie Q-M, Mani S, Zheng X-S, Li B, Li J-MJ, Guo H, Pei G-Q, An X-P, Chen JJ-W, Zhou L, Mai K-J, Wu Z-X, Li D, Anderson DE, Zhang L-B, Li S-Y, Mi Z-Q, He T-T, Cong F, Guo P-J, Huang R, Luo Y, Liu X-L, Chen JJ-W, Huang Y, Sun Q, Zhang X-L-L, Wang Y-Y, Xing S-Z, Chen Y-S, Sun Y, Li J-MJ, Daszak P, Wang L-F, Shi Z-L, Tong Y-G, Ma J-Y. 2018. Fatal swine acute diarrhoea syndrome caused by an HKU2-related coronavirus of bat origin. *Nature* 556:255–258. <https://doi.org/10.1038/s41586-018-0010-9>.
59. Reed LJ, Muench H. 1938. A simple method of estimating fifty per cent endpoints. *Am J Epidemiol* 27:493–497. <https://doi.org/10.1093/oxfordjournals.aje.a118408>.
60. Gerber PF, Xiao C-T, Lager K, Crawford K, Kulshreshtha V, Cao D, Meng X-J, Opriessnig T. 2016. Increased frequency of porcine epidemic diarrhea virus shedding and lesions in suckling pigs compared to nursery pigs and protective immunity in nursery pigs after homologous rechallenge. *Vet Res* 47:118. <https://doi.org/10.1186/s13567-016-0402-5>.
61. Miller LC, Crawford KK, Lager KM, Kellner SG, Brockmeier SL. 2016. Evaluation of two real-time polymerase chain reaction assays for *Porcine epidemic diarrhea virus* (PEDV) to assess PEDV transmission in growing pigs. *J Vet Diagn Invest* 28:20–29. <https://doi.org/10.1177/1040638715621949>.
62. Okda F, Liu X, Singrey A, Clement T, Nelson J, Christopher-Hennings J, Nelson EA, Lawson S. 2015. Development of an indirect ELISA, blocking ELISA, fluorescent microsphere immunoassay and fluorescent focus neutralization assay for serologic evaluation of exposure to North American strains of Porcine Epidemic Diarrhea Virus. *BMC Vet Res* 11:180. <https://doi.org/10.1186/s12917-015-0500-z>.